Journal of Catalysis 262 (2009) 92–101

Contents lists available at ScienceDirect

Journal of Catalysis

www.elsevier.com/locate/jcat

Thermal stability and catalytic activity of gold nanoparticles supported on silica

Gabriel M. Veith [a,*], Andrew R. Lupini [a], Sergey Rashkeev [a,b,1], Stephen J. Pennycook [a], David R. Mullins [c], Viviane Schwartz [c,d], Craig A. Bridges [c], Nancy J. Dudney [a]

[a] Materials Science and Technology Division, Oak Ridge National Laboratory, 1 Bethel Valley Rd, Oak Ridge, TN 37831, United States
[b] Physics Department, Vanderbilt University, Nashville, TN 37235, United States
[c] Chemical Sciences Division, Oak Ridge National Laboratory, Oak Ridge, TN 37831, United States
[d] Center for Nanophase Materials Sciences Division, Oak Ridge National Laboratory, Oak Ridge, TN 37831, United States

ARTICLE INFO

Article history:
Received 9 October 2008
Revised 5 December 2008
Accepted 5 December 2008
Available online 30 December 2008

Keywords:
Gold catalyst
Silica
Sputtering
Thermal stability
Tammann temperature
Titania
Gold reference catalyst
DFT calculations
Gold–support interaction

ABSTRACT

2.5 nm gold nanoparticles were grown on a fumed silica support, using the physical vapor deposition technique of magnetron sputtering, that are thermally stable when annealed in an oxygen containing environment up to at least 500 °C. Traditional Au/TiO_2 catalysts rapidly sinter to form large 13.9 nm gold clusters under these annealing conditions. This surprising stability of Au/SiO_2 is attributed to the absence of residual impurities (ensured by the halide-free production method) and a strong bond between gold and defects at the silica surface (about 3 eV per bond) estimated from density functional theory (DFT) calculations. The Au/SiO_2 catalysts are less active for CO oxidation than the prototypical Au/TiO_2 catalysts, however they can be regenerated far more easily, allowing the activity of a catalyst to be fully recovered after deactivation.

1. Introduction

Beside a high rate of activity there are many other properties that are desirable for a prospective catalyst material, including lifetime, thermal stability, and the ability to regenerate the catalyst after an undesirable loss of activity. For gold catalysts the problem of particle stability is particularly acute because gold clusters need to be very small (2–5 nm) [1–5], which results in a higher average surface energy for the gold atoms compared to those in large clusters [6]. In addition, gold clusters tend to sinter when heated due to the low Tammann temperature of gold (395 °C) which limits their operating temperatures [1,7,8]. Furthermore, local heating of the gold catalyst during a CO oxidation reaction ($\Delta G = -257$ kJ/mol$_{CO_2}$) can generate more heat than simply annealing a sample leading to enhanced particle coarsening [8,9]. Several methods to stabilize gold particles at high temperatures have been investigated including decorating Au/TiO_2 catalysts with SiO_2 [10] and confining gold in zeolitic [11] and mesoporous silica structures [12].

The majority of studies investigating heterogeneous gold catalysts have focused on gold clusters supported on reducible oxides because they tend to be the most active [13,14]. To date there is no universally accepted explanation why Au/SiO_2 catalysts are less active than the analogous Au/TiO_2 catalysts. Due to the low CO oxidation activity, and the difficulty in synthesizing gold catalysts on acidic silica, all but a few studies [12,15–30] have ignored silica and mesoporous silica supported gold catalysts. There are a number of practical benefits to using silica as a support material, such as its thermal stability, chemical inertness, excellent mechanical properties [31], and its stability in acidic environments such as those found in PEM fuel cells [4]. While it has been reported that gold clusters rapidly sinter on silica [12,31] a systematic investigation of Au/SiO_2 catalysts should enhance the understanding of the origins of catalytic activity for all gold catalysts and may facilitate the development of improved materials.

Okumura et al. provided the first tantalizing evidence that Au/SiO_2 catalysts could be very active towards CO oxidation and that the activity strongly depends on the synthesis technique [22]. They prepared Au/SiO_2 catalysts by the chemical vapor deposition (CVD) of air sensitive dimethyl gold β-ketone vapor forming a catalyst that converted 50% of a carbon monoxide gas stream around 227 K [22]. This catalyst was active at a lower temperature than gold on either TiO_2 or Al_2O_3 despite having a larger average particle

* Corresponding author. Fax: +1 865 574 4143.
E-mail address: veithgm@ornl.gov (G.M. Veith).
[1] Present address: Center for Advanced Modeling & Simulation, Idaho National Laboratory, Idaho Falls, ID 83415, United States.

0021-9517/$ – see front matter
doi:10.1016/j.jcat.2008.12.005

size [22]. Subsequent work by Daté et al. showed that introducing water to the reaction stream causes an order of magnitude increase in CO oxidation activity for the CVD prepared catalyst [27]. Despite these findings gold catalysts on non-reducible oxides, like SiO_2, are almost always less active than similar gold catalysts on reducible oxides like TiO_2 [3,13].

In this paper we show that Au nanoparticles formed on non-porous silica are active for the low-temperature oxidation of carbon monoxide and are remarkably stable against coarsening upon heating above the Tammann temperature. This study focuses on non-porous support materials to avoid confinement effects. Density Functional Theory (DFT) calculations suggest why this catalyst is more thermally stable than the titania supported gold catalyst. Compared to the benchmark Au/TiO_2 catalyst for CO oxidation distributed by the World Gold Council (WGC), this material is *more stable* but less active.

2. Methods

2.1. Catalyst preparation

The Au/SiO_2 catalysts were prepared using a magnetron sputtering technique which has been described in several previous publications [9,32,33]. A high surface area fumed silica (Cab-o-Sil) and two-1 inch Teflon® coated stir bars were placed inside a set of stainless steel (SS) cups attached to a vacuum compatible motor. A high purity gold target (Engelhard, 99.995%) was sputtered, at an applied power of 11 W, by direct current (dc) magnetron sputtering in a Ar atmosphere (research grade argon, 99.9995%—Air Liquide). The SS cups were rotated causing the powders to tumble constantly exposing a new region of the silica for the sputtered gold to deposit onto. After the deposition some material remained stuck to the sides; only 80–90% of the original material was collected. The freely tumbling catalyst was easily collected after preparation by inverting the cup onto a piece of weighing paper. Due to variations in the amount of stuck material, the weight loadings of each batch varied slightly. Deposition times were between 3–4 h. Unless noted otherwise all the tests were performed on a 6.15 wt% Au/SiO_2 catalyst.

For comparison purposes a Au/TiO_2 reference catalyst sample from the World Gold Council (Type A, Lot #02–5, prepared via deposition-precipitation, average Au particle size 3.7 nm) was evaluated under the same conditions as those used for the Au/SiO_2 samples. The Au/TiO_2 reference catalyst was stored as received in a glass vial placed in an opaque plastic container. Samples of the Au/TiO_2 were removed from the container and left in air for a minimum amount of time prior to the experiments.

2.2. Catalyst characterization

Gold loading was determined using a Thermo Jarrell Ash IRIS Inductively Coupled Plasma (ICP) Optical Emission Spectrometer. Five mL's of freshly prepared aqua-regia (3:1 mixture of hydrochloric acid and nitric acid) was used to dissolve the Au from the samples for analysis. After reacting with the aqua-regia, the samples were centrifuged to separate silica from the acid and the liquid phase was collected by decanting. Deionized water (18 MΩ) was used to wash the silica followed by the centrifuge/decanting process three more times. The collected wash was combined then diluted and used for the ICP measurements. A series of ICP standards were prepared by the serial dilution of a gold standard purchased from Alfa-Aesar.

Nitrogen BET surface area measurements were performed using a Quantachrome Instruments Autosorb 1C physisorption analyzer. Approximately 0.1 g of catalyst material was dried at 300 °C under vacuum for 4 h prior to BET measurements.

X-ray photoelectron spectroscopy (XPS) data were collected using a PHI 3056 spectrometer with a Mg anode source operated at 15 kV and an applied power of 350 W. Samples were manually pressed between two pieces of indium foil; the piece of In foil with the sample on it was then mounted to the sample holder with a piece of carbon tape (Nisshin EM Co. Ltd.). Indium was used as a support since the C1s binding energy, from adventitious carbon, was used to calibrate the binding energy shifts of the sample (C1s = 284.5 eV) [34]. High resolution data was collected at a pass energy of 5.85 eV with 0.05 eV step sizes and a minimum of 200 scans to improve the signal to noise ratio; lower resolution survey scans were collected at a pass energy of 93.5 eV with 0.5 eV step sizes and a minimum of 25 scans. The Si:Au and Ti:Au ratios were determined by comparing the Si2p, Ti2p, and Au4f photoelectron intensities above background in the high resolution data.

Powder X-ray diffraction (XRD) data were collected on the powders using a Scintag X1 diffractometer with CuK_α radiation. Samples were mounted on a glass slide with petroleum jelly. Data were collected from 10–90° 2θ over 4 h. Phase fraction analysis was performed with the program GSAS [35].

Two Scanning Transmission Electron Microscopes (STEM) were used to image the Au particles. The aberration corrected VG Microscopes HB603 UHV Scanning Transmission Electron Microscope has a resolution better than 0.8 Å and operates at 300 kV, while the Hitachi HD2000 STEM operates at 200 kV and was used for lower resolution studies. The samples were imaged in the high-angle annular dark field imaging mode (HAADF), which provides Z-contrast imaging [36], where the brightness depends on the thickness and approximately the square of the atomic number. Particle sizes were determined by measuring the widest point on the nanoparticle to account for particles that may not be orthogonal to the electron beam. Dispersion was estimated assuming each nanoparticle is hemispherical, meaning that the gold dispersion may be higher if the nanoparticles are flatter [37].

^{29}Si magic angle spinning (MAS) and cross-polarization magic angle spinning (CPMAS) solid state NMR experiments were performed to investigate the Au/SiO_2 interface. However, the Au had no detectable effect on the Si NMR signal and so those results are not included here.

X-ray absorption spectroscopy measurements were preformed at the National Synchrotron Light Source at Brookhaven National Laboratory. Data were collected on beam lines X10C and X19A. X-ray absorption near edge spectroscopy (XANES) data were collected on X10C in both transmission and fluorescence mode and compared to reference gold foil for precise energy calibration. The sample was pressed into a copper sample holder and held in place with kapton tape. Data reduction and analysis was done using the Athena/Artemis suite of programs [38].

The in situ extended X-ray absorption fine structure (EXAFS) spectroscopy measurements were performed in transmission mode using a sample pellet in a quartz tube which could be heated for sample treatments or cooled for EXAFS measurements (X19A). Approximately 150 mg of catalyst was loosely pressed into a 12 mm diameter pellet. EXAFS measurement was performed under flowing He after cooling the reactor cell to about 100 K. The program XDAP—version 3.2 was used to analyze and fit the data [39] using procedures described previously [40]. The interatomic distance r, the first nearest-neighbor coordination number (1NN), the difference of the Debye–Waller factor from the reference ($\Delta\sigma^2$), and the correction of the threshold energy (ΔE^0) were treated as free parameters during the fitting. The quality of the fit was estimated from the values of k^3 variance (V_k^3) which represents the residual between the observed and calculated spectra in the fitted range. Low values of variance indicate a good agreement between data and model.

2.3. Catalyst testing

The activity of the catalysts towards carbon monoxide oxidation was measured using both a batch reactor and a flow reactor. The batch reactor was assembled at Oak Ridge National Laboratory and consists of a standard glass infrared gas cell (10 cm optical path length, 115 cm^3 volume) with KBr windows. The change in CO and CO_2 concentrations could be measured as a function of time using a Fourier transform infrared spectrometer (FTIR). Approximately 2 mg of catalyst was spread out on a piece of aluminum foil positioned in the center of the cell so it did not obstruct the light through the cell. High purity gases (>99.99% Ar, O_2 and CO) and gas mixtures were metered and delivered to the gas cell at total flow rates of around 300 mL/min. Argon gas was flushed through the cell for 10 min prior to reaction to remove all the residual CO_2 from the atmosphere. An activated carbon filter was used to remove trace $Fe(CO)_5$ from the CO gas stream. Gas flow through the cell was manually controlled using pyrex stopcocks close to the cell body; when closed the cell pressure was 1 atm. The infrared absorbance was measured with a N_2 purged FTIR Spectrometer (BioRad 575C), equipped with a room temperature DTGS detector and KBr beamsplitter, controlled with WinIR-Pro software. Spectra were recorded at intervals of 15–60 s with 4 cm^{-1} resolution. At this resolution, 13 interferograms were averaged for 15 s time resolution. A calibration plot was created in order to relate absorbance to the concentration of the gas species. The rate of reaction could be determined by measuring the change in reactant concentration as a function of time.

A second set of activity measurements were measured using an Altramira Instruments (AIM-200) plug flow microreactor. 16.5 mg of the same Au/SiO_2 sample that was used in the FTIR batch reactor was loaded into a U-shaped quartz tube (4 mm ID) and supported with quartz wool. Catalytic activity was determined by flowing a 0.2% CO:6.4% O_2:He mixture (<4 ppm H_2O) at 50 sccm and measuring the produced CO_2. Gas exiting the reactor was analyzed with a Buck Scientific 910 gas chromatograph equipped with dual molecular sieve/porous polymer column (Alltech CTR1) and a thermal conductivity detector. The first sample was a fresh as-prepared sample with no pretreatments except for a 10 min flush of the cell with 10 mL/min of argon. The second sample was treated prior to the room temperature reaction by annealing the sample at 300 °C (ramp 10 °C/min dwell 30 min at 300 °C) in flowing argon (30 mL/min).

2.4. DFT calculations

The calculations for gold clusters attached to the SiO_2 and TiO_2 surfaces were based on Density-Functional Theory (DFT) and the generalized gradient approximation (GGA) for exchange and correlation, and plane waves [41]. First-principles calculations were performed on 4 layer-thick SiO_2 (001) quartz, 4-layer thick TiO_2 (110) rutile, and 3-layer thick (101) anatase slabs. All the slabs were terminated by non-polar surfaces; the oxygen-saturated quartz surface was fully hydrogenated. The density of free surface SiOH bonds at (001) quartz surface is 6.8/nm^2 in reasonable agreement with the experimental value of 6.3/nm^2 for fumed silica [42]. Although the morphology of the quartz surface is different from that of disordered fumed silica, the detailed surface structure plays no significant role because: (1) in any SiO_2 network, all the Si atoms are four coordinated and all the O atoms are two coordinated; (2) a small gold cluster always binds to a single anchoring site at the surface that is formed by removing a proton or an OH group (see below). Therefore, only the "local" surface structure (which is almost the same for any SiO_2 network) is important, i.e., a crystalline fully-hydrogenated quartz surface is still a reasonable model for the SiO_2 substrate. Large supercells were used (15.4 Å × 13.8 Å × 23.5 Å for quartz, 13.0 Å × 12.4 Å × 23.5 Å for rutile, and 18.9 Å × 12.7 Å × 23.5 Å for anatase) with periodic boundary conditions. The vacuum layer between slabs was >12 Å. The adsorbates and the top surface layers were fully relaxed (until quantum-mechanical forces acting on those atoms were smaller than 0.02 eV/Å), while the bottom layer was kept fixed. The surface area of the supercells was large enough to accommodate these nanoparticles and minimize inter-cluster interactions. For the DFT calculations gold nanoparticles containing N atoms, with N ranging from 1 to 35, were constructed and relaxed on the support surfaces. As it is believed that an atom by atom growth method is a dominant methodology for sputter prepared catalysts [33], the nanoparticles were constructed by adding gold atoms one at a time to the existing nanoparticles, relaxing the structure after each addition.

Table 1
Thermal stability data for Au/SiO_2 and Au/TiO_2 WGC.

Age	6.15 wt% Au/SiO_2			1.57 wt% Au/TiO_2 WGC		
	As-prepared	2W	4W	As-received	2W	4W
STEM (nm)	2.5	3.2[a]	4.8	3.7		13.9
XPS ratio[b]	0.90	0.97	0.98	19.6	37.2	44.7
BET (m^2/g)	232	–	235	73	–	39
PXD (nm)[c]	nd		6.9	nd		nd

[a] Sample post 500 °C anneal in 8% O_2/He for 1D and CO oxidation for 2D.
[b] XPS photoelectron peak, Si2p:Au4f or Ti2p:Au4f, intensity ratio.
[c] Particle size estimated from Scherrer equation, constant = 0.9 [74].

3. Results

3.1. Synthesis and characterization

The magnetron sputtering technique has several advantages for the preparation of bulk silica supported gold nanoparticles. Since no solutions are required to prepare the catalysts, the support's isoelectric point (IEP) does not constrain the synthesis conditions. No residual chloride species are left on the surface from a gold precursor and no impurities from the SS cups were detected by the ICP or XPS studies. Also, no thermal treatment or activation is required to obtain an active catalyst. One of the drawbacks of the sputter deposition process was maximum batch size. The fumed silica used in this study is non-porous (according to the *t*-method [43]) and has a N_2 BET surface area around 230 m^2/g. Because of its low freely-settled bulk density, several batches of catalysts (around 300 mg each) had to be made to have enough for all the measurements. The Au/SiO_2 samples prepared for this study were a uniform wine-red, free flowing powder. Samples with high gold loading were used to improve the characterization studies (i.e., signal/noise ratios, space velocities, etc.) however samples with lower gold loadings showed similar results.

All of the as-prepared Au/SiO_2 samples were characterized by electron microscopy. Particle size data is summarized in Table 1. A representative STEM image for a 6.15 wt% Au/SiO_2 as-deposited sample, which had been stored for 2 months in a glass vial in a $CaSO_4$ filled desiccator, is shown in Fig. 1. This sample, like all of the others examined, had a uniform distribution of gold particles (which show up as the bright spots) on the surface of the fumed silica. Analysis of the nanoparticles indicates that the average Au particle size is around 2.5 nm (55% dispersion, assuming hemispherical nanoparticles), Fig. 2. These particles are some of the smallest reported silica supported gold particles; previously published work typically shows gold particles with diameters larger than 6 nm [22,24–27]. The average projected particle separation measured from the images is less than 2 nm. Although the reduced depth of field in an aberration-corrected STEM means that particles supported at different heights go out of focus very rapidly [44],

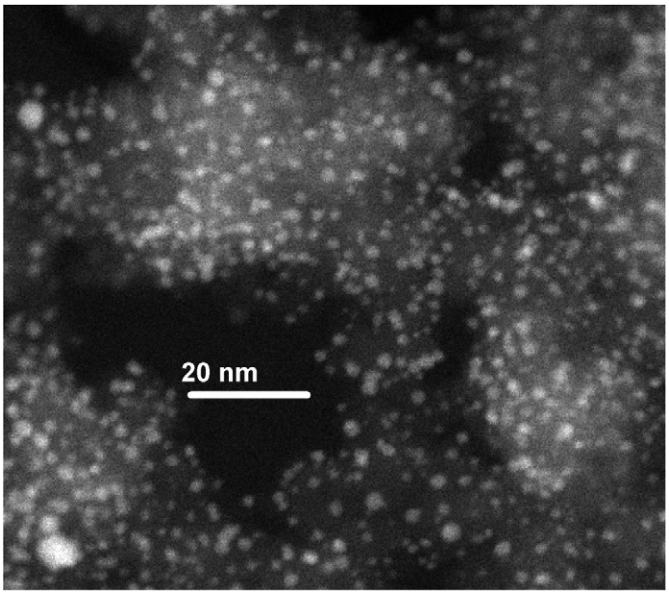

Fig. 1. Aberration corrected STEM image of as-prepared Au/SiO_2 6.15 wt%. Notice the high concentration of small gold nanoparticles (bright spots) on the silica surface.

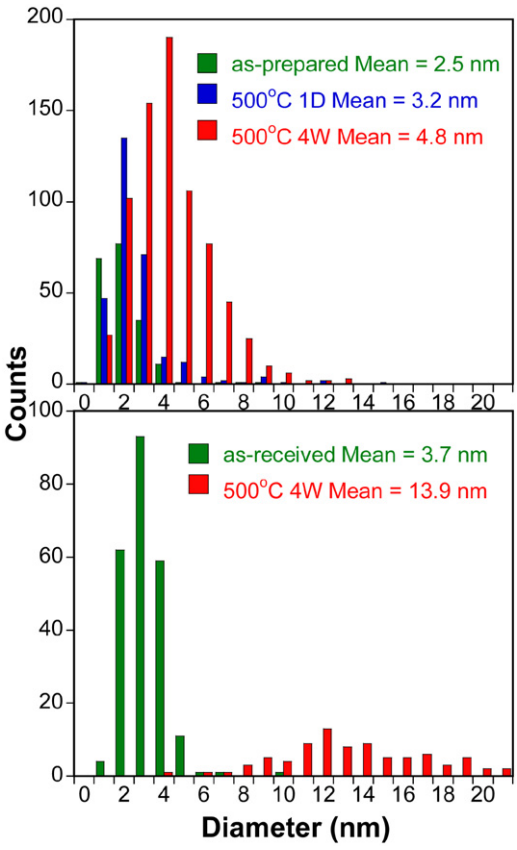

Fig. 2. (Top) Gold nanoparticle size histograms of as-prepared and thermally treated Au/SiO_2 catalysts. (Bottom) Gold nanoparticle size histograms of as-received and thermally annealed Au/TiO_2.

here the projected value provides a useful measure to compare different samples, but is probably still an underestimation of the true three-dimensional separation. STEM images of other as-deposited Au/SiO_2 samples with lower gold loadings all show a similar high concentration of 2.5 nm Au particles as well as a few larger gold particles indicating that some large particles also form during the deposition. There was no X-ray diffraction from the Au in any of

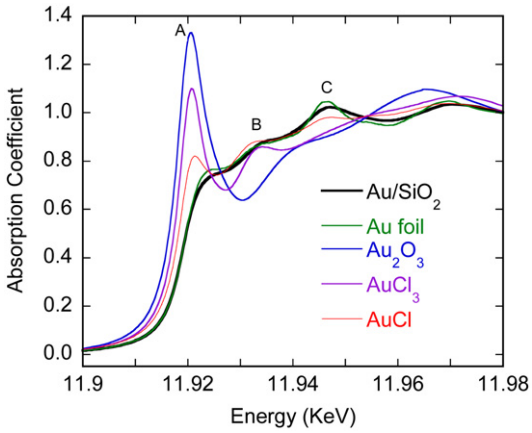

Fig. 3. XANES data of a series of Au references and as-deposited Au/SiO_2.

the as-prepared Au/SiO_2 samples. The lack of Au diffraction is most likely due to the small gold particles which lack the requisite long-range order required for diffraction.

Fig. 3 shows the Au-L_3 X-ray absorption near edge spectroscopy (XANES) data for a 5.0% Au/SiO_2 sample, two Au^{3+} references (Au_2O_3 and $AuCl_3$), a Au^+ reference (AuCl), and gold foil. The Au^{3+} species show a large absorption feature (labeled A) at a lower binding energy than the bulk gold metal. This shift to lower binding energy is due to a 2p to 5d transition which precedes the excitation to the bulk [45]. The Au^+ spectrum has a much smaller A-feature probably due to a small concentration of 5d holes. Comparing the Au/SiO_2 sample and the bulk gold foil reveals very similar shapes and edge energies, which indicates that the gold is in the metallic Au^0 state. The slight intensity reduction and increase in energy for the A, B and C features corresponds to a reduction in coordination number and a decrease in Au–Au distances consistent with the formation of gold nanoparticles [46].

The Au/SiO_2 catalysts were compared to Au/TiO_2 reference catalysts, prepared by deposition precipitation, from the World Gold Council. The Au/TiO_2 support material (Degussa P25) is a mixture of anatase and rutile phases. It has an experimentally measured surface area of 73 m^2/g and is non-porous as estimated from the *t*-method [43]. This BET surface area is slightly higher than the typically reported surface area for Degussa P25, 50 m^2/g (± 15 m^2/g) [47]. A representative STEM image and particle size analysis are shown in Figs. 4a and 2, respectively. There was a homogeneous distribution of gold clusters on the TiO_2 surface. The experimentally determined mean particle diameter was 3.7 nm which is in excellent agreement with the reported particle sizes for this catalyst.

3.2. CO oxidation

The activity of Au/SiO_2 and Au/TiO_2 were measured using a commercial flow reactor and home built batch reactor. The batch and flow reactors yield the same activity values. Catalytic activity data for the catalysts reported here and literature values for Au/SiO_2 catalysts active at ambient temperatures are presented in Tables 2 and 3, respectively. The as-prepared Au/SiO_2 catalyst shows significant catalytic activity (0.011 $mol_{CO}/(mol_{Au}\,s)$) compared to most previously reported Au/SiO_2 catalysts in the literature (0.016–0.0008 $mol_{CO}/(mol_{Au}\,s)$, Table 3). These previously reported Au/SiO_2 catalysts had significantly larger Au particles, which reduces the number of surface atoms available for reaction sites. When unused as-prepared Au/SiO_2 sample was left out in the air for 18 h and then evaluated in the batch reactor there was an order of magnitude decrease in the catalytic activity (0.001 $mol_{CO}/(mol_{Au}\,s)$). However, when this air-

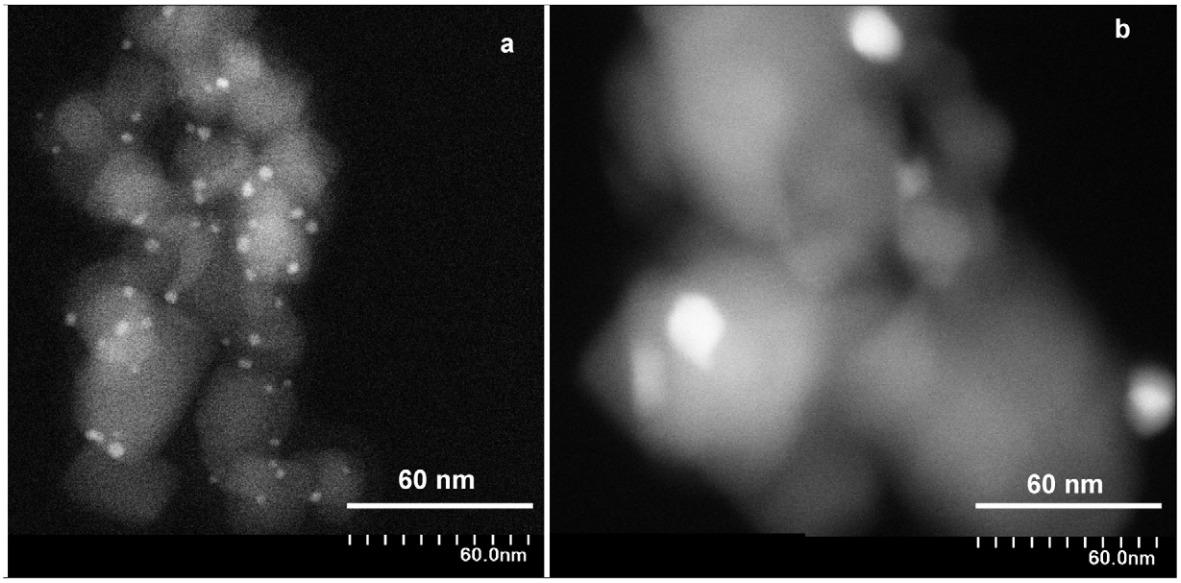

Fig. 4. (a) *Z*-contrast STEM image of as received Au/TiO_2 from the WGC and (b) *Z*-contrast STEM image of the Au/TiO_2 catalyst post 500 °C anneal in air for 4 weeks.

Table 2
Catalytic activity data for samples evaluated in this work.

Support	Au (wt%)	Particle size (nm)[a]	Activity ($mol_{CO}/(mol_{Au}\ s)$) (25 °C)	Reactor type	Comments
SiO_2	5.75	2.5	0.011	Batch[b]	Fresh sample
SiO_2	5.75	2.5	0.001	Batch[b]	Left in air
SiO_2	5.75	3.2[c]	0.019	Batch[b]	Post 400 °C air anneal 1H
SiO_2	5.75	2.5	0.011	Flow[d]	Fresh sample
SiO_2	5.75	3.2	0.019	Flow[d]	Post 300 °C 8% O_2/He anneal
SiO_2	5.75	3.2	0.004	Flow[b]	Post 4W anneal in air
TiO_2–WGC	1.56	3.7	0.298	Batch[b]	Fresh sample
TiO_2–WGC	1.56	3.7[e]	0.058	Batch[b]	Left in air
TiO_2–WGC	1.56	3.7[e]	0.060	Batch[b]	Post 400 °C air anneal 1H
TiO_2–WGC	1.56	13.9	Not detected	Flow	Post 4W anneal in air

[a] Average particle size measured from STEM data from this work.
[b] Reaction conditions: 1.5% CO/13% O_2/Ar.
[c] Size post 500 °C anneal in 8% O_2/He for 2 h. This was a higher temperature and longer duration than the annealing treatments for the catalysts used in these experiments so particle sizes are likely smaller than these reported here.
[d] Reaction conditions: 0.5% CO/0.8% O_2/50% Ar/He.
[e] Majority of the particles had diameters around 3.7 nm with larger 8–10 nm clusters evident resulting in a bimodal distribution of particles.

deactivated sample was annealed in air for an hour (400 °C), the activity recovered and was better than the as-prepared sample (0.019 $mol_{CO}/(mol_{Au}\ s)$). Attempts to thermally analyze the annealing of our deactivated catalyst with a thermogravimetric analyzer were inconclusive due to insufficient weight loss upon heating. Temperature programmed oxidation and decomposition measurements were equally inconclusive. There was no measurable loss of water or carbon containing compounds during heating in flowing gases. At this point it is not clear what processes cause the deactivation or subsequent full reactivation upon heating.

To investigate the effect of this brief annealing on catalysts structure a slightly more aggressive test was performed where the catalysts was used for a 48 h carbon monoxide oxidation test in the plug flow reactor then annealed at 500 °C for 2 h. STEM images revealed a slight coarsening of the gold nanoparticles, mean diameter 3.2 nm, Fig. 5. However the vast majority of particles (98%)

Table 3
Published ambient temperature catalytic activity data for Au on non-mesoporous SiO_2 catalysts.

Au (wt%)	Particle size (nm)	Reactivity ($mol_{CO}/(mol_{Au}\ s)$)	Preparation method	%CO:O_2 balance	*T* (°C)	Ref.
1.8	30	0.0008	IW	5% CO/5% O_2/He	40	[26]
1.0	–	0.016	IW	3.3% CO, 1.7% O_2/He	27	[28]
2.4	1.4	0.008	CVD	0.96:20:inert gas	23	[25]
2.4	1.4	0.003	CVD	0.96:20:inert gas	0	[25]
10	8.2	0.004	CVD	1% CO/air/1 ppm H_2O	0	[27]
6.6	6.6	0.004[a]	CVD	1% CO/air	0	[22]
1.4	3.5	0.057	DP—from $Au(en)_2$	1% CO/air	0	[23]
3.8	6.0	0.009	DP—from $Au(en)_2$	1% CO/air	0	[23]

[a] Extrapolated from data.

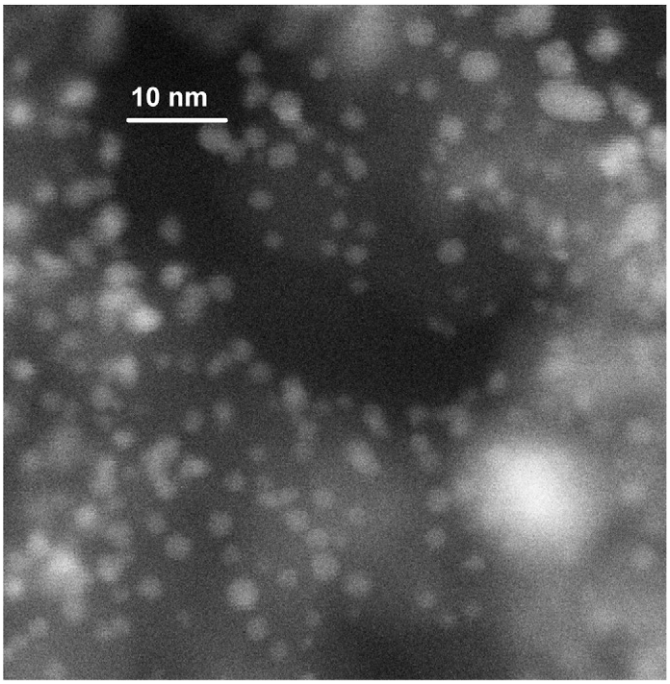

Fig. 5. *Z*-contrast STEM image of Au/SiO_2 post 1D 500 °C anneal and 48H CO oxidation test.

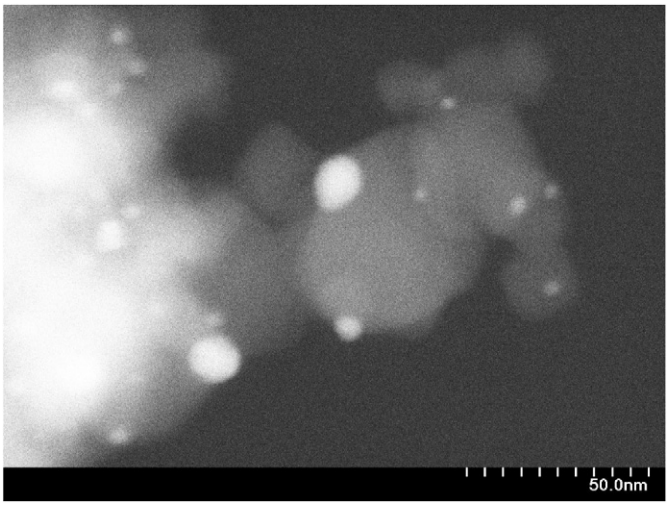

Fig. 6. *Z*-contrast STEM image of Au/TiO_2 WGC after sample left in air.

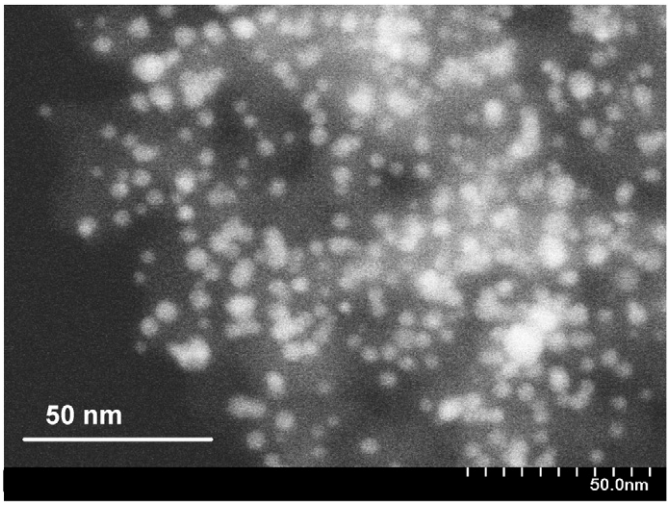

Fig. 7. *Z*-contrast STEM image of the 6.15 wt% Au/SiO_2 post 500 °C anneal for 4 weeks in air.

remain less than 3 nm in diameter and show no evidence of crystallizing into hexagonal nanoparticles. Many of the particles are still separated on average by less than 2 nm from another particle. Since some large gold clusters (>10 nm) were observed for the as-prepared Au/SiO_2 samples, it is unclear if the population of very large particles in the annealed sample increased as a result of the thermal treatments or if they were produced during the synthesis of the catalysts. There is clearly a slight amount of coarsening, but this does not seem to affect the total activity of the Au/SiO_2 catalysts.

The as-received Au/TiO_2 reference catalyst showed a significantly higher activity than the as-prepared Au/SiO_2 catalyst (0.3 vs. 0.01 $mol_{CO}/(mol_{Au}\,s)$), which is consistent with previously published catalytic data on Au/TiO_2 and Au/SiO_2 [48]. However, when the reference catalyst was left on a laboratory bench under fluorescent lights in the rather humid Tennessee air for a day there was a 5 fold decrease in its catalytic activity (Table 2). Annealing for an hour in air did not recover the activity of the reference catalyst. Thus after only a short exposure to ambient laboratory conditions, the Au/TiO_2 catalyst was found to be only 3 times more active than the annealed Au/SiO_2 catalyst. Comparing STEM images of the as-received Au/TiO_2 (Fig. 4a) and the Au/TiO_2 sample left out (Fig. 6) reveals the formation of some larger gold nanoparticles. This decrease in activity should therefore not be surprising, since the importance of small gold clusters for active gold catalysts is well known [3]. It is unclear what causes the increase in gold particle sizes when exposed to light, but reports in the literature have indicated light sensitivity of Au/TiO_2 [49].

3.3. Annealing gold catalyst

A series of annealing experiments were performed in order to understand the long term effect of thermal treatments on the structure and stability of the Au/SiO_2 and Au/TiO_2 catalysts. This data is summarized in Table 1. Samples were annealed in air at 500 °C, in the same furnace next to each other, for various times. The treated samples were then analyzed by electron microscopy, which provides a very detailed view of a small part of the sample, and by techniques that sample a much larger fraction of the material (XPS, EXAFS, PXD) to confirm that the microscopic results were representative of the material.

STEM images, at the same magnification, of the as-received and Au/TiO_2 catalyst post 4 week anneal are shown in Fig. 4; gold particle size data is presented in Fig. 2 (bottom). Annealing the Au/TiO_2 catalysts resulted in a dramatic sintering of the

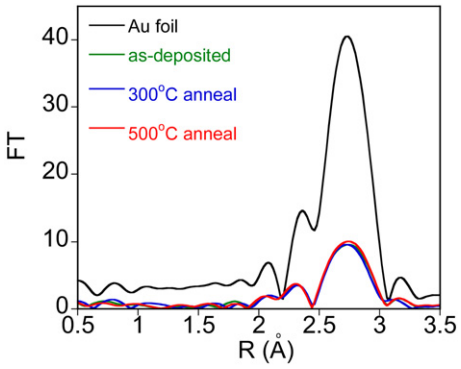

Fig. 8. EXAFS of an as-prepared 4.8 wt% Au/SiO_2 catalysts, thermally treated Au/SiO_2 catalysts and gold foil.

gold nanoparticles from an average diameter of 3.7 nm to 13.9 nm. Similar but smaller particle size increases have been reported for Au/TiO_2 annealed for shorter periods of time [50]. There was no measurable room temperature catalytic activity for the Au/TiO_2 catalysts after the four week annealing which is consistent with the formation of large inactive gold clusters.

Fig. 7 shows a STEM image of a 6.15 wt% Au/SiO_2 catalyst after it had been annealed for 4 weeks. A histogram of the annealed Au/silica particles is shown in Fig. 2. In contrast to the dramatic sintering observed for gold on TiO_2, the gold particles supported on silica coarsened only slightly from 2.5 nm to 3.2 nm (after one day) and to 4.8 nm after 28 days. Interestingly the STEM images of the annealed Au/SiO_2 catalysts reveal a very high concentration of gold clusters in close proximity to one another, with most of the gold clusters separated by distances less than the cluster diameter. The gold particles on SiO_2 are stable even after annealing in an oxygen containing environment, which has previously been shown to promote the agglomeration of gold nanoparticles at elevated temperatures [51]. After this extended annealing the Au/SiO_2 catalyst still retained about 20% of its maximum catalytic activity (0.004 $mol_{CO_{reacted}}/(mol_{Au}\,s)$).

Fig. 8 shows EXAFS data for a 4.8 wt% Au/SiO_2 sample prepared by sputtering and then heating in air first at 300 and again at 500 °C. Analysis of this EXAFS data, Table 4, show that the Au–Au distances (2.80–2.84 Å) and Au coordination numbers (7.1) do not change with thermal treatments. This confirms that there was minimal sintering and little structural change in the Au particles, even up to 500 °C, consistent with the microscopy

Table 4
EXAFS data for Au–SiO_2 catalysts.

4.8 wt% EXAFS	Au CN	R (Å)	$\Delta\sigma^2$ (10^{-4} Å^2)	ΔE^0 (eV)	ΔR	$V^3_{k\text{-fit}}$
As deposited[a]	7.1	2.84	59	−5.7	0/4	0.81
300 °C in air[a]	7.1	2.84	61	−5.1	0/4	0.82
500 °C in air[a]	7.1	2.84	58	−5.1	0/4	0.86
500 °C in air (RT scan)	7.4	2.80	111	−0.5	0/4	1.81

[a] Measured at 100 K.

data. Analysis of room temperature EXAFS data collected for 5 and 4.8 wt% samples on two different beamlines showed gold coordination numbers of 7.9 and 7.4, respectively, which confirms the batch reproducibility of this technique and the microscopy results.

The coalescence of the gold particles was further examined by XPS, which is sensitive to the surface atoms. Monitoring changes in the ratio of Si2p or Ti2p to Au4f photoelectron peak intensity as a function of time is good way to follow changes in metal particle sizes. Increases in the Si or Ti to gold ratio indicate the loss of small gold particles, which results in more of the metal oxide surface being exposed and a much lower percentage of gold atoms on the surface of a gold cluster [52]. For the Au/TiO_2 catalysts the initial Ti:Au intensity ratio starts at 19.6, Table 1. After annealing the ratio increases to 37.2 after two weeks and 44.7 after four weeks. This data confirms the loss of small gold particles and exposure of more TiO_2 surface upon annealing.

In contrast to the Au/TiO_2 data the Si:Au ratio change is much smaller and increases from 0.90 to 0.97 after two weeks then to 0.98 after four weeks. The Si:Au ratio is much smaller than the Ti:Au ratio due to the larger concentration of gold on the surface and differences in the photoelectron intensities from each support. These results indicate an appreciable coarsening of the gold particles on silica occurs within two weeks but thereafter the change is much slower with time. This conclusion supports the microscopy data which shows a rapid change in particle sizes within the first day (0.7 nm) followed by a change of only 1.6 nm over the next 27 days.

XRD studies of the annealed Au/SiO_2 catalysts showed a small peak originating from the gold clusters that was not present for the as-prepared catalysts. Analysis of the gold peak with the Sherrer equation ($\beta = 0.9$) indicated that the gold particle size was about 6.9 nm, which is consistent with the microscopy data that revealed the formation of slightly larger particles after annealing. This value is slightly larger than the value from the microscopy because this technique is biased towards detecting mainly larger particles. A Rietveld refinement study based upon powder XRD studies of the Au/TiO_2 catalysts revealed that there was an increase in the percentage of the high temperature rutile phase, from ∼15(1)% to 35(1)%, at the expense of the anatase phase due to the annealing. BET surface area analysis also indicated a loss of TiO_2 surface area, down to 39 m^2/g from 73 m^2/g, with annealing, Table 1. There was no change in the silica surface area with annealing.

3.4. DFT calculations

Calculations were performed in order to try to understand the enhanced stability of Au/SiO_2 catalysts compared to Au/TiO_2. Table 5 shows calculated binding energies for Au clusters with different numbers of gold atoms positioned on selected sites of SiO_2 and TiO_2 (rutile) surfaces. The calculated binding energy on a (110) rutile surface between Au and a two-coordinated oxygen O(2) atom is 0.8 eV, between Au and a five-coordinated Ti(5) atom is 0.4 eV, and between Au and an O(2) vacancy (shown in Table 5) is 1.2 eV. Similar binding energies (unlisted) are found for gold at the anatase (101) surface. First principle calculations show that a fully hydrogenated silica surface is inert and does not bind adsorbed Au atoms (the binding energy does not exceed 0.1 eV). However, removal of surface H or OH groups, leaving O and Si dangling bonds, forms active sites for anchoring individual gold atoms. The binding energy between Au and a surface Si dangling bond (∼3.8 eV) is higher than the binding energy between Au and an oxygen dangling bond (∼2.7 eV). These energies are higher than the binding energy of an adsorbed Au atom to any of the surface sites at the TiO_2 surface.

Table 5
Binding energies (in eV) for Au clusters with different number of gold atoms (N(Au)) attached to the dangling Si bond (for SiO_2 surface) or positioned on top of oxygen vacancy (for TiO_2 surface).

	N(Au)								
	5	8	10	12	15	20	25	30	35
SiO_2 (dangling Si)	−3.5	−3.2	−2.9	−2.7	−3.2	−2.6	−3.4	−2.7	−2.9
SiO_2 (dangling O)	−2.2	−2.4	−2.0	−2.3	−2.5	−2.1	−2.4	−2.2	−2.1
TiO_2	−1.2	−0.9	−1.6	−0.8	−1.7	−1.5	−1.1	−1.3	−1.4

The ability of O vacancies on TiO_2 substrates to anchor gold particles is well known [53] and is believed to play a possible role in the catalytic activity [54]. For TiO_2 surfaces our calculations show that the clusters are indeed anchored at an oxygen vacancy, but have a tendency to spread laterally (parallel to the surface) because some Au atoms form weaker bonds with O(2) and Ti(5) atoms located at the surface, 0.8 and 0.4 eV respectively (Fig. 9a). However, silica supported clusters have a more bulk-like, spherical shape, with only one Au atom attached to the Si dangling bond at the surface (Fig. 9b). While the calculations indicate that a dehydrogenated silica surface has the potential to form a single silica–Au bond that is stronger than a single titania–Au bond there probably are several Au–SiO_2 bonds in the larger experimentally observed clusters with several hundred atoms. The binding energy of such a larger cluster is nearly proportional to the number of its Au/SiO_2 bonds to the substrate, i.e., larger clusters bind to the surface even stronger (and are more unlikely to sinter) than smaller ones.

4. Discussion

4.1. Thermal stability of gold catalysts

The experimental evidence clearly shows that the Au/SiO_2 catalysts are more stable at elevated temperatures than the more commonly studied Au/TiO_2 catalysts. The temperatures used in these experiments are well above the Tammann temperature for gold (395 °C) where metal mobility becomes significant [7]. There are a number of differences between the silica and titania supported nanoparticles but these differences should be detrimental to Au/SiO_2 stability. The Au/SiO_2 catalysts have a higher weight loading compared to Au/TiO_2 (6.15 wt% vs. 1.57 wt%), the Au gold nanoparticles on silica are smaller, and they are separated by much shorter distances (projected separation typically less than 3 nm) than the analogous titania supported nanoparticles. Since smaller particles are structurally unstable and the separations are reduced, the smaller particles would be expected to have a higher probability of becoming mobile and combining [6]. Even after annealing at high temperatures for four weeks, the Au/SiO_2 particles are still separated by distances less than 3 nm. In comparison, the gold particles supported on TiO_2 coalesced much more rapidly, despite being separated by much larger distances, than the SiO_2 supported clusters.

As noted previously there was a 50% loss of TiO_2 surface area and a near doubling of the fraction of rutile in the support material due to sintering, while no similar changes were observed for SiO_2. It is unknown what effect these bulk changes in the TiO_2 will have on the nanoparticle stability, since reorganizing the TiO_2

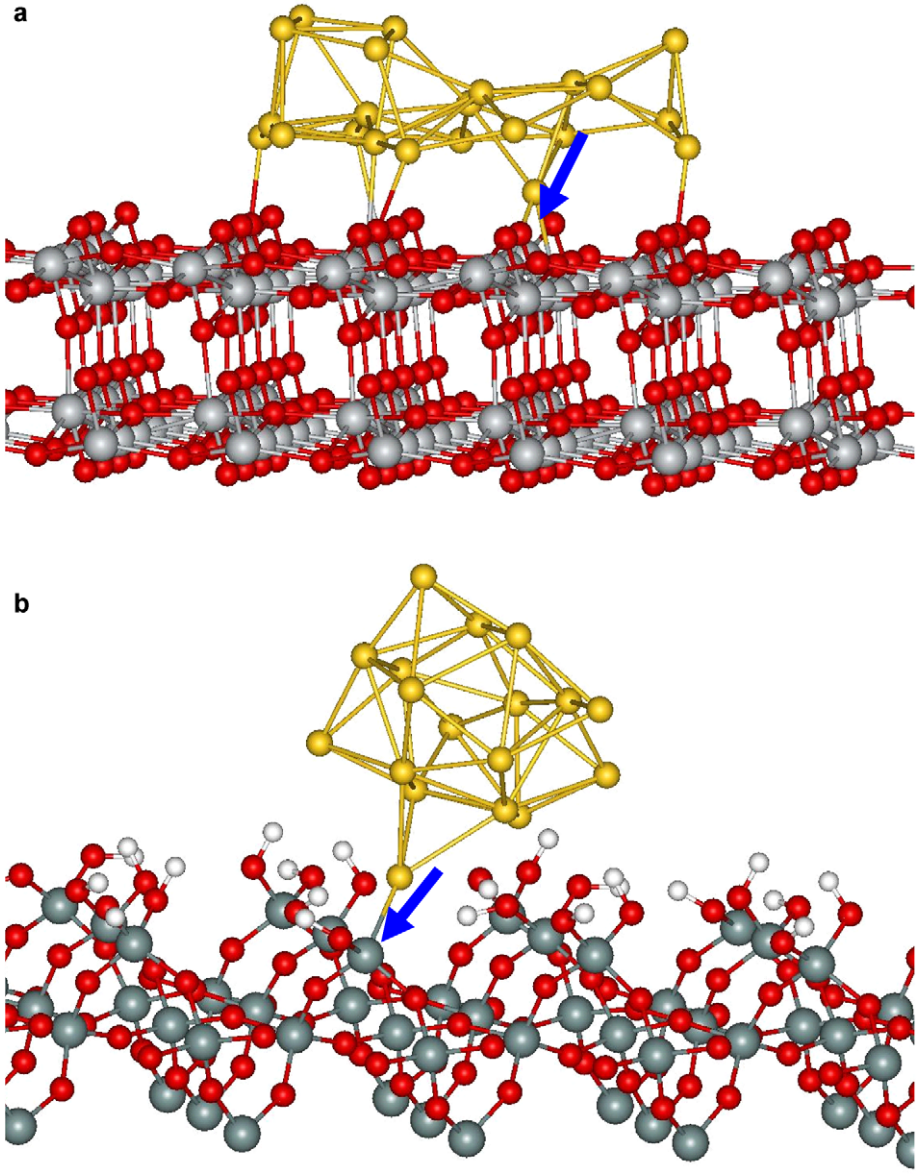

Fig. 9. (a) 21-atom Au cluster positioned on top of an oxygen vacancy at the TiO_2 anatase (101) surface; (b) 18-atom Au cluster attached to a single Si dangling bond at the SiO_2 quartz (001) surface. Gold atoms are shown in yellow, oxygen—in red, hydrogen—in white, Ti—in light gray; Si—in gray. The surface anchoring sites (O vacancy for TiO_2 and dangling Si atom for SiO_2) are indicated by blue arrows. (For interpretation of the references to color in this figure legend, the reader is referred to the web version of this article.)

structure is likely to facilitate the Au migration. In addition, higher temperatures are likely to promote the formation and migration of oxygen vacancies, which have been reported to be important for stabilizing gold nanoparticles [55–59]. The exact mechanism of the supported nanoparticle growth under these conditions is clearly an area that requires further study.

4.2. Origin of gold stability

In order to understand the enhanced stability of gold/silica catalysts several experimental efforts to characterize the metal-silica interface using EXAFS and solid state ^{29}Si-NMR were attempted but thus far have been unsuccessful. Therefore we turned to first principles DFT calculations to explain the origin of this stability.

The DFT calculations performed in this study indicate that protons or –OH groups on the silica surface need to be removed in order to form a strong Au–silica interaction. Although the sputtered Au atoms are deposited at thermal energies, given the well known high energy tail present in the distribution of sputtered species [60,61], there may be enough kinetic energy from a fraction of the incident Ar or Au atoms to remove surface protons or surface hydroxyl groups enabling the formation of the strong Au–support bond.

From DFT calculations it is generally agreed that gold atoms do not bind strongly to a stoichiometric TiO_2 surface [62–64]. Previous DFT work indicates that gold atoms bond much stronger to defective, reduced or non-stoichiometric TiO_2 surfaces [50,56,63,65,66]. The average calculated Au binding energy to oxygen defect sites found in the present work is 1.2 eV, which is in good agreement with previously reported calculated values of: 1.6 eV for a reduced rutile surface [50], 1.2 eV for one vacancy site [65], and 1.7 eV for an O point defect in a 1×3 cell [67]. Compared to Au/TiO_2 there are relatively few theoretical studies investigating Au/SiO_2 catalysts and these rely on unrealistic models of the surface. Previous DFT studies of Au/SiO_2 assumed that SiO_2 adopted

a rutile rather than quartz structure [66,68]. Laursen and Linic reported that the interactions between a gold bilayer and a reduced rutile–SiO_2 surface are weaker (−1.07 eV/vacancy) than comparable interactions on a reduced TiO_2 surface (−1.97 eV) [66]. Liu et al. similarly reported lower binding energies between Au and reduced rutile–SiO_2 (2.25 eV) as compared to Au and reduced TiO_2 (2.87 eV) [68].

The experimental results presented in this study clearly demonstrate the important role that the support plays in the stabilization of the nanoparticles on bulk support materials. Modeling the gold–SiO_2 support interactions using an improved model (quartz structure and a hydrogen passivated surface) produced a theoretical model which correlates well with the experimental data. Similar to the modeling of Au/TiO_2 we find that in order to stabilize the gold clusters on silica a surface defect needs to be formed. Unlike the gold nanoparticles reported in this study, silica supported gold catalyst prepared from $HAuCl_4$ precursors are reported to be thermally unstable and poorly bound, resulting in the rapid agglomeration of gold nanoparticles into large gold clusters along with a concomitant loss of catalytic activity [69–71]. Based on the modeling presented above it is reasonable to believe the origin of this instability is the inability of precipitation techniques to adequately remove hydroxyl or proton groups during the preparation processes. Recently, thermal stability of Au on silica was also demonstrated by Zhu et al. who reported that gold particles prepared by $Au(en)_2^+$ and confined in mesoporous silica maintained a 5 nm particle size even at 500 °C [21]. Zhu et al. performed their deposition at a pH 10, i.e. when the silica surface is deprotonated forming a $Si–O^-$ dangling bond where the gold precursor bound [21].

4.3. Catalytic activity

Despite the formation of gold particles with similar diameters, the Au/SiO_2 prepared in this study was significantly less active for CO oxidation than Au/TiO_2. The literature involving gold catalysts contains many examples of gold catalysts being more active on reducible support materials versus non-reducible support materials, which is consistent with our present work. However, there are also examples where gold catalysts supported on Al_2O_3 are more active [72], as active, or only a factor of ∼2 less active than highly active Au/TiO_2 catalysts [13], indicating that this simple model of reducible oxides being better supports may not be the whole story. The DFT calculations performed in this study produced gold clusters on SiO_2 that were more spherical than those on TiO_2, which could spread out laterally on the TiO_2 surface. It is possible that the more spherical nature of Au on SiO_2 may lead to the loss of the perimeter reaction pathway, which is important for Au/TiO_2 catalysts [3], and the reduction in total oxidation rate may be due to the loss of perimeter sites.

Deactivation of gold catalysts on a number of support materials has been reported. Konova et al. reported the deactivation of a Au/TiO_2 catalyst proceeds by two mechanisms; the adsorption of CO from the reaction gas in the form of carbonates and coarsening of the gold particles due to heating [73]. Our Au/SiO_2 samples deactivate when they are left out in the air. Such a deactivation is not typically reported in the literature. The Au/SiO_2 catalysts can be fully reactivated by annealing with little change in the catalysts structure. It is clear that during the extended annealing experiments there is a growth of the gold clusters, however, unlike the inactive Au/TiO_2 catalysts, the Au/SiO_2 catalysts retain a level of activity due to the stability of the gold nanoparticles on silica. This activity is still larger than the activity of Au/SiO_2 catalysts left in air (0.004 versus 0.001 $mol_{CO_{reacted}}/(mol_{Au}\,s)$).

5. Conclusions

A new way to prepare silica supported catalysts has been reported. These catalysts are structurally stable when heated in air to 500 °C for several weeks or during a CO oxidation reaction. While both Au/SiO_2 and the reference Au/TiO_2 catalysts were observed to deactivate when they are exposed to air, the Au/SiO_2 catalyst was easily reactivated by a brief heating with no apparent coarsening or loss of activity. In fact there appeared to be an increase in activity for the briefly annealed Au/SiO_2. Exposure of the Au/TiO_2 catalyst to atmospheric conditions resulted in a 5 fold decrease in activity, attributed to agglomeration of the Au particles. Our DFT results suggest that the origin of the Au/SiO_2 stability appears to be due to the strong binding of the Au nanoparticles to defects on the silica surface. The binding energy between Au and silica was significantly larger than any simple binding energy between Au and titania. Defects are formed by the removal of surface hydrogen or OH groups by the energetic gold atoms deposited during the deposition process. The ability to easily reactivate the catalyst, thermal stability, and the unique gold–support interactions make this material worthy of further study.

Acknowledgments

The authors thank Professor Craig Barnes and Dr. Jason Clarke (University of Tennessee Chemistry Department) for collecting and analyzing the ^{29}Si-NMR data, Ben Jang (University Texas, Commerce) and Wenfu Yan (ORNL) for assistance with some catalytic measurements as well as Steven Overbury (ORNL) and Sokrates Pantelides (Vanderbilt) for many helpful discussions. The calculation portion of this work is supported in part by a grant of computer time from the DoD High Performance Computing Modernization Program at the Maui High Performance Computer Center (MHPCC), Naval Oceanographic Office (NAVO) and the U.S. Army Engineer Research and Development Center (ERDC). A portion of this research (Hitachi STEM) was conducted at the Center for Nanophase Materials Sciences, which is sponsored at Oak Ridge National Laboratory by the Division of Scientific User Facilities, U.S. Department of Energy. Use of the National Synchrotron Light Source, Brookhaven National Laboratory, was supported by the U.S. Department of Energy, Office of Science, Office of Basic Energy Sciences, under Contract No. DE-AC02-98CH10886. This research was also sponsored by the U.S. Department of Energy's Office of Basic Energy Sciences, Division of Materials Sciences and Engineering (G.M.V., A.R.L., S.J.P., C.A.B., N.J.D.), and the Division of Chemical Sciences (D.R.M., V.S.).

References

[1] M. Haruta, CATTECH 6 (2002) 102.
[2] M. Haruta, Chem. Record 3 (2003) 75.
[3] M. Haruta, Gold Bull. 37 (2004) 27.
[4] M. Haruta, J. New Mater. Electrochem. Syst. 7 (2004) 163.
[5] A.S.K. Hashmi, G.J. Hutchings, Angew. Chem. Int. Ed. 45 (2006) 7896.
[6] G. Schmid, in: B. Corain, G. Schmid, N. Toshima (Eds.), Metal Nanoclusters in Catalysis and Materials Science, part 1, Elsevier, Amsterdam, 2008, p. 3.
[7] S. Golunski, Platinum Metals Rev. 51 (2007) 162.
[8] M.B. Cortie, E. van der Lingen, Mater. Forum 26 (2002) 1.
[9] G.M. Veith, A.R. Lupini, S.J. Pennycook, G.W. Ownby, N.J. Dudney, J. Catal. 231 (2005) 151.
[10] H. Zhu, Z. Ma, S.H. Overbury, S. Dai, Catal. Lett. 116 (2007) 128.
[11] T.M. Salama, T. Shido, H. Minagawa, M. Ichikawa, J. Catal. 152 (1995) 322.
[12] J.P. Gabaldon, M. Bore, A.K. Datye, Top. Catal. 44 (2007) 253.
[13] M.C. Kung, R.J. Davis, H.H. Kung, J. Phys. Chem. C 111 (2007) 11767.
[14] M.M. Schubert, S. Hackenberg, A.C. van Veen, M. Muhler, V. Plzak, R.J. Behm, J. Catal. 197 (2001) 113.
[15] G. Budroni, A. Corma, Angew. Chem. Int. Ed. 45 (2006) 3328.
[16] C. Yang, M. Kalwei, F. Schüth, K.-j. Chao, Appl. Catal. A 254 (2003) 289.
[17] M. Okumura, S. Tsubota, M. Iwamoto, M. Haruta, Chem. Lett. 27 (1998) 315.

[18] A. Ghosh, C.R. Patra, P. Mukherjee, M. Sastry, R. Kumar, Microporous Mesoporous Mater. 58 (2003) 201.
[19] C.-W. Chiang, A. Wang, B.-Z. Wan, C.-Y. Mou, J. Phys. Chem. B 109 (2005) 18042.
[20] D.B. Akolekar, G. Foran, S.K. Bhargava, J. Synch. Rad. 11 (2004) 284.
[21] H. Zhu, C. Liang, W. Yan, S.H. Overbury, S. Dai, J. Phys. Chem. B 110 (2006) 10842.
[22] M. Okumura, S. Nakamura, S. Tsubota, T. Nakamura, M. Azuma, M. Haruta, Catal. Lett. 51 (1998) 53.
[23] H. Zhu, Z. Ma, J.C. Clark, Z. Pan, S.H. Overbury, S. Dai, Appl. Catal. A 326 (2007) 89.
[24] G. Martra, L. Prati, C. Manfredotti, S. Biella, M. Rossi, S. Coluccia, J. Phys. Chem. B 107 (2003) 5453.
[25] S. Schimpf, M. Lucas, C. Mohr, U. Rodemerck, A. Brücker, J. Radnik, H. Hofmeister, P. Claus, Catal. Today 72 (2002) 63.
[26] S.D. Lin, M. Bollinger, M.A. Vannice, Catal. Lett. 17 (1993) 245.
[27] M. Daté, M. Okumura, S. Tsubota, M. Haruta, Angew. Chem. Int. Ed. 43 (2004) 2129.
[28] N. Weiher, E. Bus, L. Delannoy, C. Louis, D.E. Ramaker, J.T. Miller, J.A. van Bokhoven, J. Catal. 240 (2006) 100.
[29] R. Zanella, A. Sandoval, P. Santiago, V.A. Basiuk, J.M. Saniger, J. Phys. Chem. B 110 (2006) 8559.
[30] J.T. Miller, A.J. Kropf, Y. Zha, J.R. Regalbuto, L. Delannoy, C. Louis, E. Bus, J.A. van Bokhoven, J. Catal. 240 (2006) 222.
[31] K. Zhu, J. Hu, R. Richards, Catal. Lett. 100 (2005) 195.
[32] G.M. Veith, A.R. Lupini, S.J. Pennycook, N.J. Dudney, in: E. Gaigneaux (Ed.), in: Studies in Surface Science and Catalysis, vol. 71, Elsevier, Amsterdam, 2006, pp. 71–78.
[33] G.M. Veith, A.R. Lupini, S.J. Pennycook, A. Villa, L. Prati, N.J. Dudney, Catal. Today 122 (2007) 248.
[34] J.F. Moulder, W.F. Stickle, P.E. Sobol, K.D. Bomben, Handbook of X-Ray Photoelectron Spectroscopy, Perkin–Elmer, Eden Prairie, MN, 1992.
[35] A.C. Larson, R.B. von Dreele, GSAS-Generalized Crystal Structure Analysis System, 1987.
[36] S.J. Pennycook, P.D. Nellist, in: D.G. Rickerby, U. Valdré, G. Valdré (Eds.), Impact of Electron and Scanning Probe Microscopy on Materials Research, Kluwer Academic, Dordrecht, 1999, p. 166.
[37] A. Carlsson, A. Puig-Molina, T.V.W. Janssens, J. Phys. Chem. B 110 (2006) 5286.
[38] B. Ravela, M. Newville, J. Synch. Rad. 12 (2005) 537.
[39] M. Vaarkamp, J.C. Linders, D.C. Koningsberger, Physica B 209 (1995) 159.
[40] S.H. Overbury, V. Schwartz, D.R. Mullins, W. Yan, S. Dai, J. Catal. 241 (2006) 56.
[41] M.C. Payne, M.P. Teter, D.C. Allan, T.A. Arias, J.D. Joannopoulos, Rev. Mod. Phys. 64 (1992) 1045.
[42] C.C. Liu, G.E. Maciel, Anal. Chem. 68 (1996) 1401.
[43] S. Lowell, J.E. Sheilds, M.A. Thomas, M. Thommes, Characterization of Porous Solids and Powders: Surface Area, Pore Size and Density, Springer, Dordrecht, 2004.
[44] A.Y. Borisevich, A.R. Lupini, S.J. Pennycook, Proc. Natl. Acad. USA 103 (2006) 3044.
[45] J.W. Watkins II, R.C. Elder, B. Greene, D.W. Darnall, Inorg. Chem. 26 (1987) 1147.
[46] R.E. Benfield, D. Grandjean, M. Kröll, R. Pugin, T. Sawitowski, G. Schmid, J. Phys. Chem. B 105 (2001) 1961.
[47] A. Mills, S. Le Hunte, J. Photochem. Photobiol. A 108 (1997) 1.
[48] A. Wolf, F. Schüth, Appl. Catal. A Gen. 226 (2002) 1.
[49] R. Zanella, C. Louis, Catal. Today 107–108 (2005) 768.
[50] N. Lopez, J.K. Norskov, T.V.W. Janssens, A. Carlsson, A. Puig-Molina, B.S. Clausen, J.-D. Grunwaldt, J. Catal. 225 (2004) 86.
[51] C.C. Chusuei, X. Lai, K. Luo, D.W. Goodman, Top. Catal. 14 (2001) 71.
[52] A. Frydman, D.G. Castner, M. Schmal, C.T. Campbell, J. Catal. 157 (1995) 133.
[53] E. Wahlström, N. Lopez, R. Schaub, P. Thostrup, A. Ronnau, C. Africh, E. Laegsgaard, J.K. Norskov, F. Besenbacher, Phys. Rev. Lett. 90 (2003) 026101.
[54] I.N. Remediakis, N. Lopez, J.K. Norskov, Appl. Catal. A 291 (2005) 13.
[55] J.A. Rodríguez, G. Liu, T. Jirsak, J. Hrbek, Z. Chang, J. Dvorak, A. Maiti, J. Am. Chem. Soc. 124 (2002) 5242.
[56] E. Wahlström, N. Lopez, R. Schaub, P. Thostrup, A. Rønnau, C. Africh, E. Lægsgaard, J.K. Nørskov, F. Besenbacher, Phys. Rev. Lett. 90 (2003) 026101.
[57] M.S. Chen, D.W. Goodman, Top. Catal. 44 (2007) 41.
[58] F. Sedona, M. Sambi, L. Artiglia, G.A. Rizzi, A. Vittadini, A. Fortunelli, G. Granozzi, J. Phys. Chem. C 112 (2008) 3187.
[59] D. Matthey, J.G. Wang, S. Wendt, J. Matthiesen, R. Schaub, E. Laegsgaard, B. Hammer, F. Besenbacher, Science 315 (2007) 1692.
[60] P.R. Willmott, Prog. Surf. Sci. 76 (2004) 163.
[61] G.M. Turner, I.S. Falconer, B.W. James, D.R. McKenzie, J. Vac. Sci. Technol. A 10 (1992) 455.
[62] N. Lopez, J.K. Nørskov, Surf. Sci. 515 (2002) 175.
[63] K. Okazaki, S. Ichikawa, Y. Maeda, M. Haruta, M. Kohyama, Appl. Catal. A Gen. 291 (2005) 45.
[64] L.M. Liu, B. McAllister, H.Q. Ye, P. Hu, J. Am. Chem. Soc. 128 (2006) 4017.
[65] A. Vijay, G. Mills, H. Metiu, J. Chem. Phys. 118 (2003) 6536.
[66] S. Laursen, S. Linic, Phys. Rev. Lett. 97 (2006) 026101.
[67] Y. Wang, G.S. Hwang, Surf. Sci. 542 (2003) 72.
[68] Z.-P. Liu, S.J. Jenkins, D.A. King, Phys. Rev. Lett. 93 (2004) 156102.
[69] L.B. Ortiz-Soto, O.S. Alexeev, M.D. Amiridis, Langmuir 22 (2006) 3112.
[70] M.P. Casaletto, A. Longo, A.M. Venezia, A. Martorana, A. Prestianni, Appl. Catal. A 302 (2006) 309.
[71] M.A.P. Dekkers, M.J. Lippits, B.E. Nieuwenhuys, Catal. Today 54 (1999) 381.
[72] M. Comotti, W.-C. Li, B. Spliethoff, F. Schüth, J. Am. Chem. Soc. 128 (2006) 917.
[73] P. Konova, A. Naydenov, C. Venkov, D. Mehandjiev, D. Andreeva, T. Tabakova, J. Mol. Catal. A Chem. 213 (2004) 235.
[74] B.D. Cullity, Elements of X-Ray Diffraction, second ed., Addison–Wesley, Reading, 1978.